## MARTIAN GEOLOGY

# Radar evidence of subglacial liquid water on Mars

R. Orosei[1]*, S. E. Lauro[2], E. Pettinelli[2], A. Cicchetti[3], M. Coradini[4], B. Cosciotti[2],
F. Di Paolo[1], E. Flamini[4], E. Mattei[3], M. Pajola[5], F. Soldovieri[6], M. Cartacci[3],
F. Cassenti[7], A. Frigeri[3], S. Giuppi[3], R. Martufi[7], A. Masdea[8], G. Mitri[9], C. Nenna[10],
R. Noschese[3], M. Restano[11], R. Seu[7]

The presence of liquid water at the base of the martian polar caps has long been suspected but not observed. We surveyed the Planum Australe region using the MARSIS (Mars Advanced Radar for Subsurface and Ionosphere Sounding) instrument, a low-frequency radar on the Mars Express spacecraft. Radar profiles collected between May 2012 and December 2015 contain evidence of liquid water trapped below the ice of the South Polar Layered Deposits. Anomalously bright subsurface reflections are evident within a well-defined, 20-kilometer-wide zone centered at 193°E, 81°S, which is surrounded by much less reflective areas. Quantitative analysis of the radar signals shows that this bright feature has high relative dielectric permittivity (>15), matching that of water-bearing materials. We interpret this feature as a stable body of liquid water on Mars.

T he presence of liquid water at the base of the martian polar caps was first hypothesized more than 30 years ago (1) and has been inconclusively debated ever since. Radio echo sounding (RES) is a suitable technique to resolve this dispute, because low-frequency radars have been used extensively and successfully to detect liquid water at the bottom of terrestrial polar ice sheets. An interface between ice and water, or alternatively between ice and water-saturated sediments, produces bright radar reflections (2, 3). The Mars Advanced Radar for Subsurface and Ionosphere Sounding (MARSIS) instrument on the Mars Express spacecraft (4) is used to perform RES experiments (5). MARSIS has surveyed the martian subsurface for more than 12 years in search of evidence of liquid water (6). Strong basal echoes have been reported in an area close to the thickest part of the South Polar Layered Deposits (SPLD), Mars' southern ice cap (7). These features were interpreted as due to the propagation of the radar signals through a very cold layer of pure water ice having negligible attenuation (7). Anomalously bright reflections were subsequently detected in other areas of the SPLD (8).

On Earth, the interpretation of radar data collected above the polar ice sheets is usually based on the combination of qualitative (the morphology of the bedrock) and quantitative (the reflected radar peak power) analyses (3, 9). The MARSIS design, particularly the very large footprint (~3 to 5 km), does not provide high spatial resolution, strongly limiting its ability to discriminate the presence of subglacial water bodies from the shape of the basal topography (10). Therefore, an unambiguous detection of liquid water at the base of the polar deposit requires a quantitative estimation of the relative dielectric permittivity (hereafter, permittivity) of the basal material, which determines the radar echo strength.

Between 29 May 2012 and 27 December 2015, MARSIS surveyed a 200-km-wide area of Planum Australe, centered at 193°E, 81°S (Fig. 1), which roughly corresponds to a previous study area (8). This area does not exhibit any peculiar characteristics, either in topographic data from the Mars Orbiter Laser Altimeter (MOLA) (Fig. 1A) (11, 12) or in the available orbital imagery (Fig. 1B) (13). It is topographically flat, composed of water ice with 10 to 20% admixed dust (14, 15), and seasonally covered by a very thin layer of $CO_2$ ice that does not exceed 1 m in thickness (16, 17). In the same location, higher-frequency radar observations performed by the Shallow Radar instrument on the Mars Reconnaissance Orbiter (18) revealed barely any internal layering in the SPLD and did not detect any basal echo (fig. S1), in marked contrast with findings for the North Polar Layer Deposits and other regions of the SPLD (19).

A total of 29 radar profiles were acquired using the onboard unprocessed data mode (5) by transmitting closely spaced radio pulses centered at either 3 and 4 MHz or 4 and 5 MHz (table S1). Observations were performed when the spacecraft was on the night side of Mars to minimize ionospheric dispersion of the signal. Figure 2A shows an example of a MARSIS radargram collected in the area, where the sharp surface reflection is followed by several secondary reflections produced by the interfaces between layers within the SPLD. The last of these echoes represents the reflection between the ice-rich SPLD and the underlying material (hereafter, basal material). In most of the investigated area, the basal reflection is weak and diffuse, but in some locations, it is very sharp and has a greater intensity (bright reflections) than the surrounding areas and the surface (Fig. 2B). Where observations from multiple orbits overlap, the data acquired at the same frequency have consistent values of both surface and subsurface echo power (fig. S2).

The two-way pulse travel time between the surface and basal echoes can be used to estimate the depth of the subsurface reflector and map the basal topography. Assuming an average signal velocity of 170 m/μs within the SPLD, close to that of water ice (20), the depth of the basal reflector is about 1.5 km below the surface. The large size of the MARSIS footprint and the diffuse nature of basal echoes outside the bright reflectors prevent a detailed reconstruction of the basal topography, but a regional slope from west to east is recognizable (Fig. 3A). The subsurface area where the bright reflections are concentrated is topographically flat and surrounded by higher ground, except on its eastern side, where there is a depression.

The permittivity, which provides constraints on the composition of the basal material, can in principle be retrieved from the power of the reflected signal at the base of the SPLD. Unfortunately, the radiated power of the MARSIS antenna is unknown because it could not be calibrated on the ground (owing to the instrument's large dimensions), and thus the intensity of the reflected echoes can only be considered in terms of relative quantities. It is common to normalize the intensity of the subsurface echo to the surface value (21)—i.e., to compute the ratio between basal and surface echo power. Such a procedure has the advantage of also compensating for any ionospheric attenuation of the signal. Following this approach, we normalized the subsurface echo power to the median of the surface power computed along each orbit; we found that all normalized profiles at a given frequency yield consistent values of the basal echo power (fig. S3). Figure 3B shows a regional map of basal echo power after normalization; bright reflections are localized around 193°E, 81°S in all intersecting orbits, outlining a well-defined, 20-km-wide subsurface anomaly.

To compute the basal permittivity, we also require information about the dielectric properties of the SPLD, which depend on the composition and temperature of the deposits. Because the exact ratio between water ice and
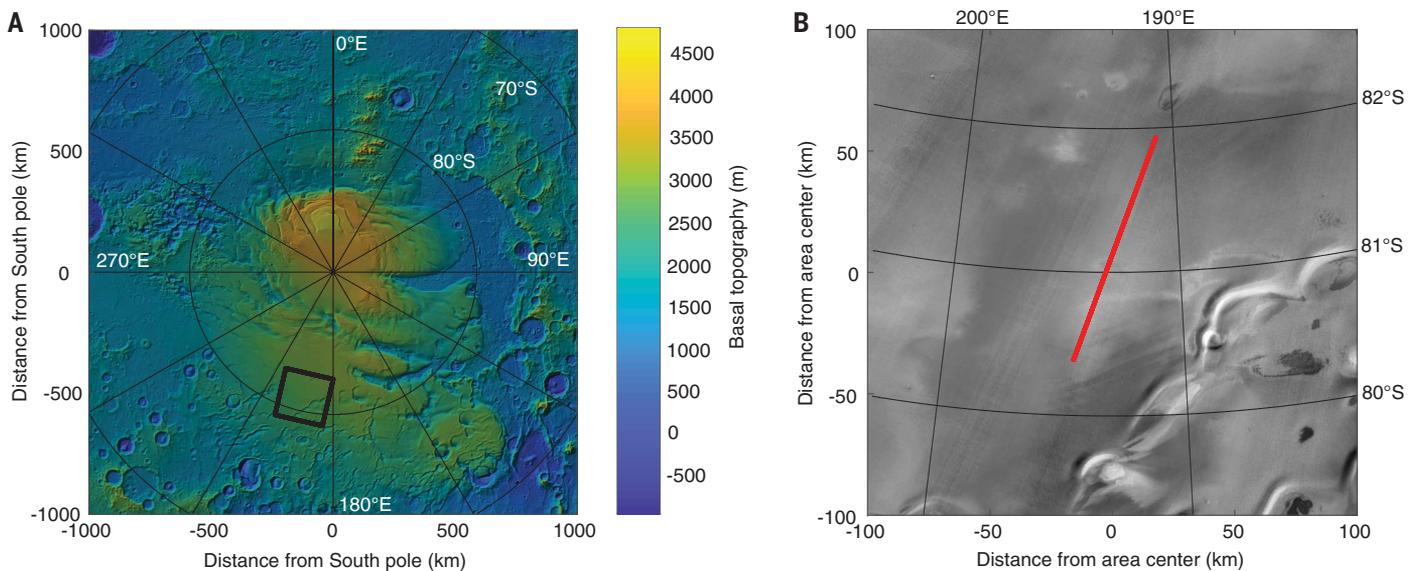
**Fig. 1. Maps of the investigated area.** (**A**) Shaded relief map of Planum Australe, Mars, south of 75°S latitude. The map was produced using the MOLA topographic dataset (*11*). The black square outlines the study area. (**B**) Mosaic produced using infrared observations by the THEMIS (Thermal Emission Imaging System) camera (*13*), corresponding to the black square in (A). South is up in the image. The red line marks the ground track of orbit 10737, corresponding to the radargram shown in Fig. 2A. The area consists mostly of featureless plains, except for a few large asymmetric polar scarps near the bottom right of (B), which suggest an outward sliding of the polar deposits (*34*).

dust is unknown (*15*), and because the thermal gradient between the surface and the base of the SPLD is poorly constrained (*22*), we explored the range of plausible values for such parameters and computed the corresponding range of permittivity values. The following general assumptions were made: (i) The SPLD is composed of a mixture of water ice and dust in varying proportions (from 2 to 20%), and (ii) the temperature profile inside the SPLD is linear, starting from a fixed temperature at the surface (160 K) and rising to a variable temperature at the base of the SPLD (range, 170 to 270 K). Various electromagnetic scenarios were computed (*5*) by considering a plane wave impinging normally onto a structure with three layers: a semi-infinite layer with the permittivity of free space, a homogeneous layer representing the SPLD, and another semi-infinite layer representing the material beneath the SPLD, with variable permittivity values. The output of this computation is an envelope encompassing a family of curves that relate the normalized basal echo power to the permittivity of the basal material (Fig. 4A). This envelope is used to determine the distribution of the basal permittivity (inside and outside the bright area) by weighting each admissible value of the permittivity with the values of the probability distribution of the normalized basal echo power (Fig. 4B). This procedure generated two distinct distributions of the basal permittivity estimated inside and outside the bright reflection area (Fig. 4C and fig. S4), whose median values at 3, 4, and 5 MHz are 30 ± 3, 33 ± 1, and 22 ± 1 and 9.9 ± 0.5, 7.5 ± 0.1, and 6.7 ± 0.1, respectively. The basal permittivity outside the bright area is in the range of 4 to 15, typical for dry terrestrial volcanic rocks. It is also in agreement with pre-

vious estimates of 7.5 to 8.5 for the material at the base of the SPLD (*23*) and with values derived from radar surface echo power for dense dry igneous rocks on the martian surface at mid-latitudes (*24, 25*). Conversely, permittivity values as high as those found within the bright area have not previously been observed on Mars. On Earth, values greater than 15 are seldom associated with dry materials (*26*). RES data collected in Antarctica (*27*) and Greenland (*9*) show that a permittivity larger than 15 is indicative of the presence of liquid water below polar deposits. On the basis of the evident analogy of the physical phenomena on Earth and Mars, we can infer that the high permittivity values retrieved for the bright area below the SPLD are due to (partially) water-saturated materials and/or layers of liquid water.

We examined other possible explanations for the bright area below the SPLD (supplementary text). For example, a $CO_2$ ice layer at the top or the bottom of the SPLD, or a very low temperature of the $H_2O$ ice throughout the SPLD, could enhance basal echo power compared with surface reflections. We reject these explanations (supplementary text), either because of the very specific and unlikely physical conditions required, or because they do not cause sufficiently strong basal reflections (figs. S5 and S6). Although the pressure and the temperature at the base of the SPLD would be compatible with the presence of liquid $CO_2$, its relative dielectric permittivity is much lower (about 1.6) (*28*) than that of liquid water (about 80), so it does not produce bright reflections.

The substantial amounts of magnesium, calcium, and sodium perchlorate in the soil of the northern plains of Mars, discovered using the

Phoenix lander's Wet Chemistry Lab (*29*), support the presence of liquid water at the base of the polar deposits. Perchlorates can form through different physical and/or chemical mechanisms (*30, 31*) and have been detected in different areas of Mars. It is therefore reasonable to assume that they are also present at the base of the SPLD. Because the temperature at the base of the polar deposits is estimated to be around 205 K (*32*), and because perchlorates strongly suppress the freezing point of water (to a minimum of 204 and 198 K for magnesium and calcium perchlorates, respectively) (*29*), we therefore find it plausible that a layer of perchlorate brine could be present at the base of the polar deposits. The brine could be mixed with basal soils to form a sludge or could lie on top of the basal material to form localized brine pools (*32*).

The lack of previous radar detections of subglacial liquid water has been used to support the hypothesis that the polar caps are too thin for basal melting and has led some authors to state that liquid water may be located deeper than previously thought [e.g., (*33*)]. The MARSIS data show that liquid water can be stable below the SPLD at relatively shallow depths (about 1.5 km), thus constraining models of Mars' hydrosphere. The limited raw-data coverage of the SPLD (a few percent of the area of Planum Australe) and the large size required for a meltwater patch to be detectable by MARSIS (several kilometers in diameter and several tens of centimeters in thickness) limit the possibility of identifying small bodies of liquid water or the existence of any hydraulic connection between them. Because of this, there is no reason to conclude that the presence of subsurface water on Mars is limited to a single location.
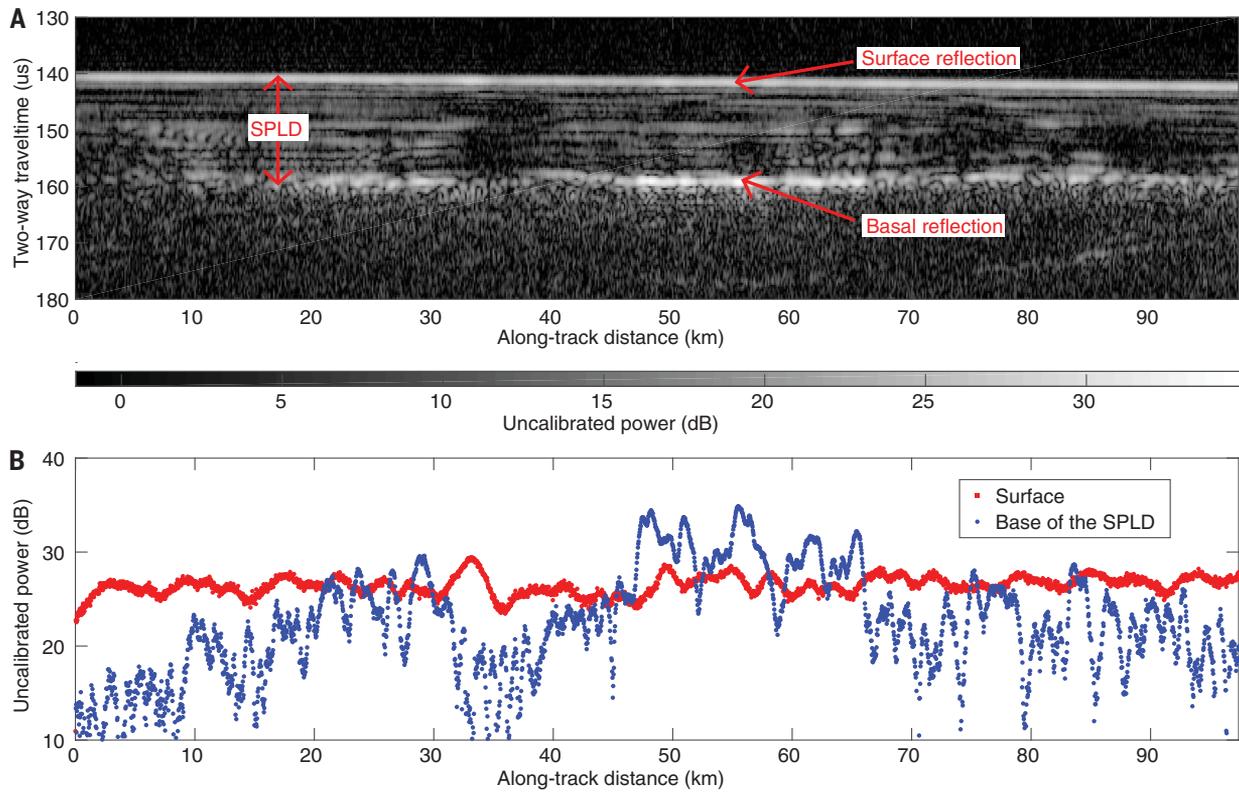
**Fig. 2. Radar data collected by MARSIS.** (**A**) Radargram for MARSIS orbit 10737, whose ground track is shown in Fig. 1B. A radargram is a bi-dimensional color-coded section made of a sequence of echoes in which the horizontal axis is the distance along the ground track of the spacecraft, the vertical axis represents the two-way travel time of the echo (from a reference altitude of 25 km above the reference datum), and brightness is a function of echo power. The continuous bright line in the topmost part of the radargram is the echo from the surface interface, whereas the bottom reflector at about 160 μs corresponds to the SPLD/basal material interface. Strong basal reflections can be seen at some locations, where the basal interface is also planar and parallel to the surface. (**B**) Plot of surface and basal echo power for the radargram in (A). Red dots, surface echo power; blue dots, subsurface echo power. The horizontal scale is along-track distance, as in (A), and the vertical scale is uncalibrated power in decibels. The basal echo between 45 and 65 km along-track is stronger than the surface echo even after attenuation within the SPLD.
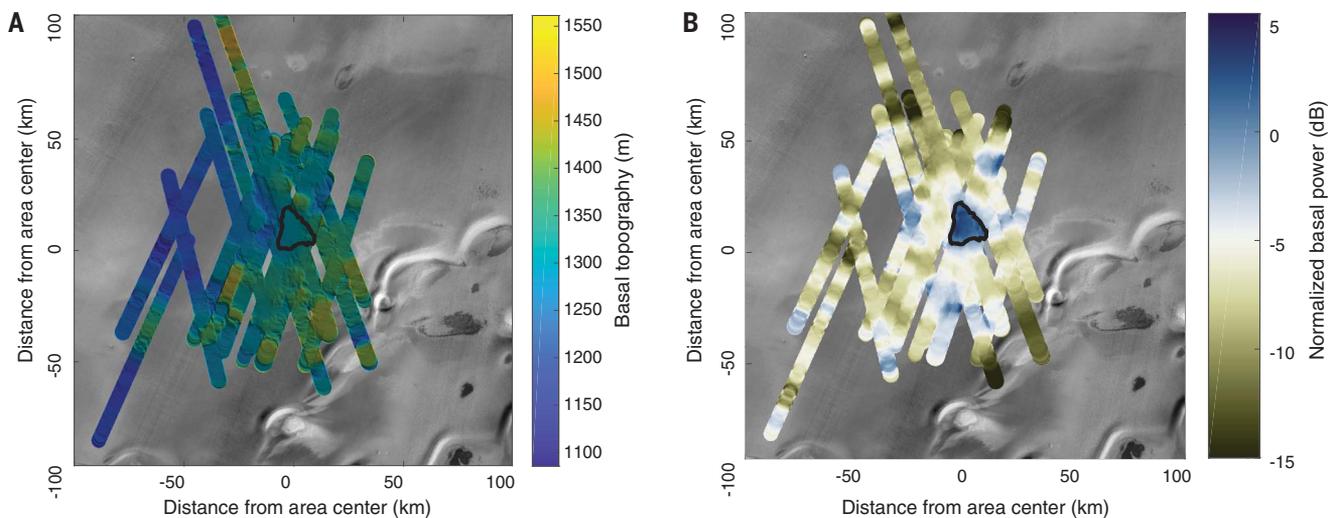


**Fig. 3. Maps of basal topography and reflected echo power.** (**A**) Color-coded map of the topography at the base of the SPLD, computed with respect to the reference datum. The black contour outlines the area in which bright basal reflections are concentrated. (**B**) Color-coded map of normalized basal echo power at 4 MHz. The large blue area (positive values of the normalized basal echo power) outlined in black corresponds to the main bright area; the map also shows other, smaller bright spots that have a limited number of overlapping profiles. Both panels are superimposed on the infrared image shown in Fig. 1B, and the value at each point is the median of all radar footprints crossing that point.
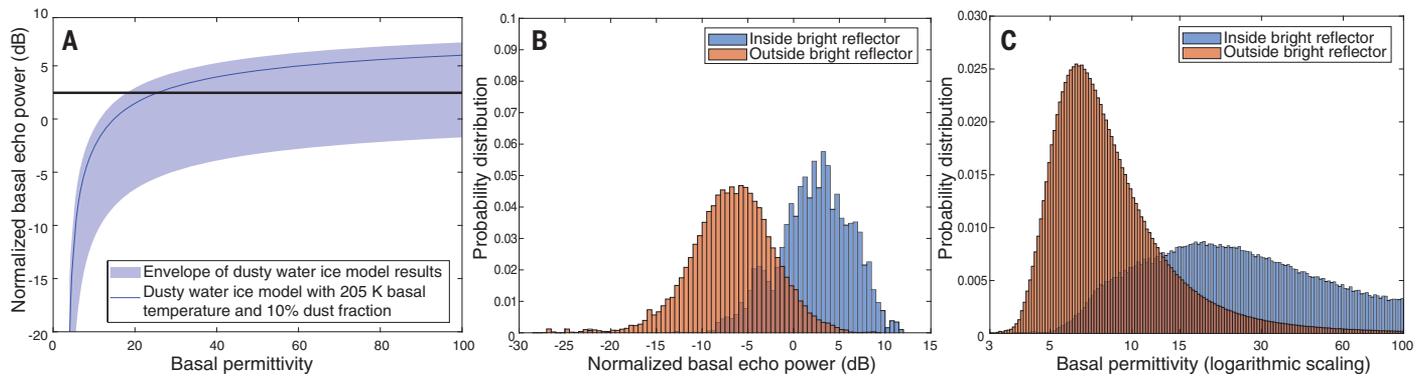
**Fig. 4. Results of the simulation and retrieved permittivities.**
(**A**) Output of the electromagnetic simulations computed at 4 MHz (figs. S4 and S6). The blue shaded area is the envelope of all curves incorporating different amounts of $H_2O$ ice and dust along with various basal temperatures for the SPLD. The blue line is the curve for a single model (basal temperature of 205 K and 10% dust content), shown for illustration, and the black horizontal line is the median normalized basal echo power at 4 MHz from the observations. (**B**) Normalized basal echo power distributions inside (blue) and outside (brown) the bright reflection area, indicating two distinct populations of values. These distributions, together with the chart in (A), are used to compute the basal permittivity; for example, the intersection between the blue curve and the black line gives a basal permittivity value of 24. (**C**) Basal permittivity distributions inside (blue) and outside (brown) the bright reflection area. The nonlinear relationship between the normalized basal echo power and the permittivity produces an asymmetry (skewness) in the distributions of the values.

**REFERENCES AND NOTES**

1. S. M. Clifford, *J. Geophys. Res.* **92**, 9135–9152 (1987).
2. D. W. Ashmore, R. G. Bingham, *Antarct. Sci.* **26**, 758–773 (2014).
3. S. P. Carter et al., *Geochem. Geophys. Geosyst.* **8**, 3016 (2007).
4. G. Picardi et al., *Science* **310**, 1925–1928 (2005).
5. Materials and methods are available as supplementary materials.
6. W. M. Farrell et al., *Geophys. Res. Lett.* **36**, L15206 (2009).
7. J. J. Plaut et al., *Science* **316**, 92–95 (2007).
8. M. Cartacci, A. Frigeri, R. Orosei, E. Pettinelli, paper presented at the American Geophysical Union Fall Meeting, San Francisco, CA, 15 to 19 December 2008.
9. G. K. A. Oswald, S. P. Gogineni, *J. Glaciol.* **54**, 94–106 (2008).
10. M. J. Siegert, S. Carter, I. Tabacco, S. Popov, D. D. Blankenship, *Antarct. Sci.* **17**, 453–460 (2005).
11. D. E. Smith et al., *J. Geophys. Res.* **106**, 23689–23722 (2001).
12. G. A. Neumann et al., *Geophys. Res. Lett.* **30**, 1561 (2003).
13. C. S. Edwards et al., *J. Geophys. Res. Planets* **116**, E10008 (2011).
14. M. T. Zuber et al., *Science* **317**, 1718–1719 (2007).
15. J. Li et al., *J. Geophys. Res. Planets* **117**, E04006 (2012).
16. M. L. Litvak et al., *J. Geophys. Res. Planets* **112**, E03S13 (2007).
17. O. Aharonson et al., *J. Geophys. Res. Planets* **109**, E05004 (2004).
18. R. Seu et al., *J. Geophys. Res. Planets* **112**, E05S05 (2007).
19. R. Seu et al., *Science* **317**, 1715–1718 (2007).
20. E. Pettinelli et al., *Rev. Geophys.* **53**, 593–641 (2015).
21. S. E. Lauro et al., *Geophys. Res. Lett.* **37**, L14201 (2010).
22. M. A. Wieczorek, *Icarus* **196**, 506–517 (2008).
23. Z. Zhang et al., *J. Geophys. Res. Planets* **113**, E05004 (2008).
24. L. M. Carter et al., *Geophys. Res. Lett.* **36**, L23204 (2009).
25. J. Mouginot et al., *Icarus* **210**, 612–625 (2010).
26. Y. Guéguen, V. Palciauskas, *Introduction to the Physics of Rocks* (Princeton Univ. Press, 1994).
27. M. E. Peters, D. D. Blankenship, D. L. Morse, *J. Geophys. Res. Solid Earth* **110**, B06303 (2005).
28. A. A. Maryott, E. R. Smith, Table of Dielectric Constants of Pure Liquids (no. NBS-514, National Bureau of Standards, 1951).
29. M. H. Hecht et al., *Science* **325**, 64–67 (2009).
30. D. C. Catling et al., *J. Geophys. Res. Planets* **115**, E00E11 (2010).
31. Y. S. Kim, K. P. Wo, S. Maity, S. K. Atreya, R. I. Kaiser, *J. Am. Chem. Soc.* **135**, 4910–4913 (2013).
32. D. A. Fisher, M. H. Hecht, S. P. Kounaves, D. C. Catling, *J. Geophys. Res. Planets* **115**, E00E12 (2010).
33. J. Lasue et al., *Space Sci. Rev.* **174**, 155–212 (2013).
34. C. Grima et al., *Icarus* **212**, 96–109 (2011).
35. R. Orosei, A. Cicchetti, Data files and electromagnetic simulation software used in the paper "Radar evidence of subglacial liquid water on Mars." Zenodo (2018); doi: 10.5281/zenodo.1285179.

# Science

## Radar evidence of subglacial liquid water on Mars

R. Orosei, S. E. Lauro, E. Pettinelli, A. Cicchetti, M. Coradini, B. Cosciotti, F. Di Paolo, E. Flamini, E. Mattei, M. Pajola, F. Soldovieri, M. Cartacci, F. Cassenti, A. Frigeri, S. Giuppi, R. Martufi, A. Masdea, G. Mitri, C. Nenna, R. Noschese, M. Restano and R. Seu

### Liquid water under Mars' southern ice cap

Mars is known to host large quantities of water in solid or gaseous form, and surface rocks show clear evidence that there was liquid water on the planet in the distant past. Whether any liquid water remains on Mars today has long been debated. Orosei *et al.* used radar measurements from the Mars Express spacecraft to search for liquid water in Mars' southern ice cap (see the Perspective by Diez). They detected a 20-km-wide lake of liquid water underneath solid ice in the Planum Australe region. The water is probably kept from freezing by dissolved salts and the pressure of the ice above. The presence of liquid water on Mars has implications for astrobiology and future human exploration.

*Science*, this issue p. 490; see also p. 448

| | |
|---|---|
| ARTICLE TOOLS | http://science.sciencemag.org/content/361/6401/490 |
| SUPPLEMENTARY MATERIALS | http://science.sciencemag.org/content/suppl/2018/07/24/science.aar7268.DC1 |
| RELATED CONTENT | http://science.sciencemag.org/content/sci/361/6400/320.full<br>http://science.sciencemag.org/content/sci/361/6401/448.full |
| REFERENCES | This article cites 42 articles, 6 of which you can access for free<br>http://science.sciencemag.org/content/361/6401/490#BIBL |
| PERMISSIONS | http://www.sciencemag.org/help/reprints-and-permissions |

Use of this article is subject to the Terms of Service